Identification of the rail radiation using beamforming and a 2 D array

Florent Le Courtois, Jean-Hugh Thomas, Franck Poisson, Jean-Claude Pascal

ACOUSTICS 2012

Identification of the rail radiation using beamforming and a 2 D array

F. Le Courtois[a], J.-H. Thomas[b], F. Poisson[a] and J.-C. Pascal[b]

[a]Innovation et recherche SNCF, 40 avenue des terroirs de France, 75012 Paris
[b]Laboratoire d'acoustique de l'université du Maine, Bât. IAM - UFR Sciences Avenue Olivier Messiaen 72085 Le Mans Cedex 9
florent.lecourtois@gmail.com

Rolling noise is a major contribution to the train pass-by noise. Array processing provides maps of the sources of the train. The rolling noise contribution is located on the wheels at 2 kHz on these maps and the rail is not well identified as a source, whereas its acoustical contribution can be in the same order of magnitude as the wheel contribution in the medium frequency range (1000 Hz).
A bending wave causes the rail to radiate in a particular direction due to different wavespeeds in the air and in the rail. Beamforming processing identifies this acoustical radiation only under particular conditions, which is an explanation to the underestimation of the rail radiation on the global noise map of the train.
This article presents a simple radiation model of the rail and the simulation result provided from beamforming processing to localize the theoretical radiation angle. An experimentation is performed using the classical 2D array designed for train pass-by source localization. The rail is excited in the vertical direction using a shaker. The radiation angle is not retrieved: the use of this classical array is not relevant to measure the radiation angle.

1 Introduction

In rolling situation, roughnesses on the wheel and rail surfaces cause a relative displacement between these elements. It generates wheel, rail and sleeper vibrations. The acoustical radiation of those vibrations is called rolling noise. Track Wheels Interaction Noise Software (TWINS) [1, 2] is used for acoustical prediction of the rolling noise. For example, on a French high speed track, the emitted noise level of the rail, the wheels of a TGV and the sleepers are plotted in Figure 1 in dB(A) integrated during a train wheel pass-by time for a listening point at 1 m from the track. The rail is identified as the main contribution to rolling noise on a wide frequency band [600 2000] Hz.

Beamforming is an array processing used to provide noise

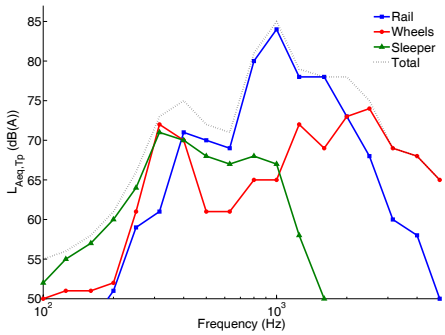

Figure 1: TWINS estimation of the acoustic contributions of sleepers, rail and wheels during the pass-by of the train at 1m.

maps of the train and identify the sources [3]. Results of the beamforming can be presented in one-third octave band cartographies, as shown in Figure 2, for the 1272 Hz centered band. Noise sources seem to be identified at the wheel-rail contact point. The rail is not clearly identified as a source.

Kitagawa and Thompson [4, 5] explain that the rail is not

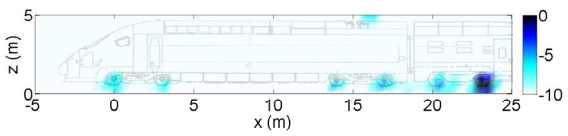

Figure 2: Acoustic map of a TGV for the one-third octave band centered on 1272 Hz. The results are presented in a normalized dB scale.

detected (or underestimated) due to a particular radiation angle which beamforming processing is not able to identify in this case. This article presents an acoustic radiation model of the rail. Then beamforming is introduced and applied on this rail radiation model. An experiment is settled on a real rail with a classical array used for sound source characterization on the train.

2 Model of the rail radiation

The railway track is composed of a steel rail, a pad and a concrete sleepers, the whole lies on a ballast layer. Several models of the track dynamics had been developed. The RODEL model [1, 2] is the simplest one proposed in TWINS. It was validated in [6].

2.1 Vibratory behavior of the track

In the RODEL model, the rail is represented by an infinite Timoshenko beam. The pads and sleepers are assumed to be close enough so that their periodic location is approximated by a continuous layer. The pads are assimilated to a damped spring layer and the sleepers to a mass layer. The ballast effect is also represented by a damped spring layer. Each layer is simply supported by the underneath one.

Considering an harmonic force $F = F_0 \exp(j2\pi f_0 t)$ applied in $x_0 = 0$ m, the vertical motions of the rail, u, and the sleepers, w, are described by three dynamical equations [2]:

$$GA\kappa \frac{\partial}{\partial x}\left(\phi - \frac{\partial u}{\partial x}\right) + \tilde{K}_s(u-w) + m_r' \frac{\partial^2 u}{\partial t^2} = F\delta(x-x_0), \quad (1)$$

$$GA\kappa\left(\phi - \frac{\partial u}{\partial x}\right) + \rho I \frac{\partial^2 \phi}{\partial t^2} - EI\frac{\partial^2 \phi}{\partial x^2} = 0, \quad (2)$$

and

$$m_s' \frac{\partial^2 w}{\partial t^2} = \tilde{K}_s'(u-w) - \tilde{K}_b' w. \quad (3)$$

I is the rotation moment, κ is the shear modulus and m_r' the linear mass of the rail. G is the shear modulus of the steel

$$G = \frac{E}{2+2\nu}, \quad (4)$$

where ν and E are the Poisson coefficient and the Young modulus of the steel. $\tilde{K}$ is an equivalent stiffness for the double layer pad-ballast

$$\tilde{K}(\omega) = \frac{\tilde{K}_p(\tilde{K}_b - \omega^2 m_s')}{\tilde{K}_p + \tilde{K}_b - \omega^2 m_s'}, \quad (5)$$

with $\tilde{K}_p$ and $\tilde{K}_b$ the stiffnesses of the pad and the ballast and $m_s^{'}$ the linear mass of the sleeper. $\tilde{K}_p$ and $\tilde{K}_b$ are complex values

$$\tilde{K}_p = K_p(1 + j\eta_p) \text{ and } \tilde{K}_b = K_b(1 + j\eta_b) \quad (6)$$

to take into account damping.
Equations 1, 2 and 3 lead to two wavenumber values. One corresponds to an evanescent wave and will be neglected. The propagating wavenumber is written with a real and an imaginary part

$$\tilde{k}_x = k_x + j\alpha. \quad (7)$$

α is the attenuation coefficient of the wave and k_x the propagating part.
For the French high speed railway track, the parameter values are given in the table 1 [2]. Numerical values of k_x and α are plotted in Figure 3, as a function of the frequency. The attenuation coefficient presents a maximum around 250 Hz and decreases below 1 m^{-1} after 500 Hz.

Parameter	Symbol	Value	Unit
Rail moment of inertia	I	$20,18 \times 10^{-6}$	[m^4]
Rail density	ρ	7850	[$kg.m^{-3}$]
Rail transversal section	A	$6,48 \times 10^{-3}$	[m^2]
Rail loss factor	η_r	0,02	[-]
Rail Shear Coefficient	κ	0,4	[-]
Steel Poisson coefficient	ν	0,3	[-]
Steel Young modulus	E	$2,1 \times 10^{11}$	[Pa]
Linear pad stiffness	K_s	300	[$MN.m^{-2}$]
Pad loss factor	η_s	0,2	[-]
Linear sleeper mass	$m_t^{'}$	250	[$kg.m^{-1}$]
Linear ballast stiffness	K_b	100	[$MN.m^{-2}$]
Ballast loss factor	η_b	1,0	[-]

Table 1: Parameters and their values for a French high speed railway track.

The vertical accelerances of the rail, H_{rail}, and of the sleeper, $H_{sleeper}$, are also calculated from equations 1, 2 and 3. The accelerance is the ratio of the acceleration and a unitary force. Both accelerances are plotted in Figure 4. Below 500 Hz, H_{rail} decreases greatly. $H_{sleeper}$ is neglectable compared to H_{rail}.
The rail velocity in x is given by

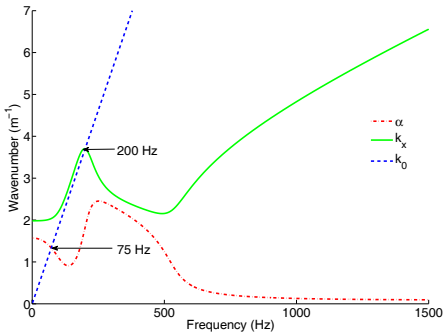

Figure 3: Real part, k_x, (green) and imaginary part, α, (red) of the calculated wavenumber of a bending wave in the rail. The acoustical wavenumber is plotted in blue.

$$v(x) = V_0 \begin{cases} \exp(-jk_x x)e^{(-\alpha x)} & \text{if } x > 0 \\ \exp(jk_x x)e^{(\alpha x)} & \text{if } x < 0 \end{cases} \quad (8)$$

for an excitation in $x_0 = 0$. V_0 is the speed amplitude of the rail at the excitation point, it can be calculated using the accelerance values

$$V_0(f) = \frac{H_{rail}(f)}{j2\pi f} F_0, \quad (9)$$

assuming that $F_0 = 1$ Pa.

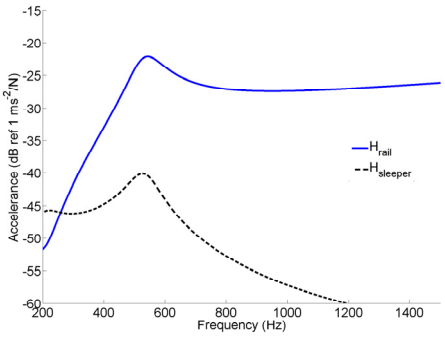

Figure 4: Accelerance of the rail, H_{rail}, and of the sleeper, $H_{sleeper}$, calculated for a French high speed track.

2.2 Acoustical model

Let assume the speed continuity of the particules at the fluid structure interface. For a fast numerical computation, the rail model is composed of a line of N_i acoustical monopoles, as in Figure 5. The model was developped in [4] and improved in [7]. The pressure received at a listening point m is then

$$p_m(k_0) = j\rho_0 c k_0 \sum_{i=1}^{N_i} \frac{Q_i}{4\pi r_{mi}} e^{(-jk_0 r_{mi})}, \quad (10)$$

with r_{mi} the i^{th} monopole-listening point distance, Q_i the flow velocity of the i^{th} monopole. ρ_0 and c are, respectively, the density of the air and the sound celerity in the air and k_0 the acoustical wavenumber.
The discretisation imposes some constraint to ensure the convergence of the calculated pressure. The monopole number N_i for the model of rail radiation is chosen to ensure a 60 dB decrease on the vibration amplitude from the excitation point to the farthest monopole [5].

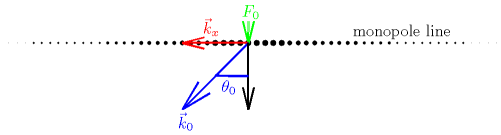

Figure 5: Representation of a rail excited in F_0 by a monopole line. The model radiates in the angle θ_0.

The pressure level, calculated in equation 10, should not depend on the number of monopoles N_i. For the i^{th} monopole located in x_i, the amplitude is

$$Q_i = v(x_i)S_0, \quad (11)$$

with S_0 as the equivalent surface of the rail represented by the monopole.

2.3 Acoustic behavior of the model

In Figure 3, for $k_0 > k_x$, the acoustic sound waves are evanescent due to an acoustic short-circuit. The sound wave is propagating above 200 Hz.
The phase delay between the excitation point and the i^{th} monopole is

$$\text{Phase}(Q_i) = -k_x x_i. \tag{12}$$

This delay leads to a constructive and destructive phase summation of the monopole line; the acoustic power is radiated in a particular direction characterized by the angle

$$\theta_0 = \text{asin}\left(\frac{k_x}{k_0}\right), \tag{13}$$

shown in Figure 5. This angle is plotted in Figure 6 as a function of the frequency. 90 ° is the direction parallel to the rail and 0 ° is the direction perpendicular to the monopole line.

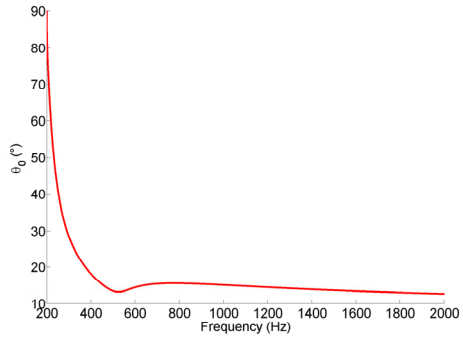

Figure 6: Radiation angle of the rail model calculated for a high speed track.

2.4 Limitations of the model

The model is quite simple and based on physical criteria, but several limitations have to be mentioned:

- S_0 is quite difficult to estimate, a quantitative use of the model is restricted;
- the sleepers periodicity is not taken into account for calculation facilities;
- the monopole line model radiation presents a symetrical rotation around its center.

3 Beamforming

Beamforming consists in listening to a particular direction of arrival (DOA), using a microphone array, in order to localize acoustical sources. The DOA is characterized by the angles θ_i and ϕ_i, the azimut and the elevation, defined with regard to the center of the array, as presented in Figure 7.
For an array of M microphones, $\mathbf{p}$ is the Fourier transform of the M measurements at the frequency f. $\mathbf{p}$ is a $[M \times 1]$ vector. Let introduce a delay for an incoming plane wave in $[\theta_i\ \phi_i]$ for the m^{th} microphone

$$\tau_{mi} = \frac{-x_m \sin\theta_i \cos\phi_i - z_m \sin\phi_i}{c} \tag{14}$$

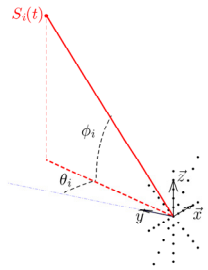

Figure 7: Definition of coordinates θ and ϕ, azimut and elevation, with regard to the center of a microphone array.

whith x_m and z_m the microphone coordinates and R the distance between the array and the rail. τ_{mi} represents a propagating delay between the m^{th} sensors of the array for a plane sound wave at the frequency f incoming from the direction $[\theta_i\ \phi_i]$. The average of the delayed sensor signals gives an estimation of the sound amplitude in this direction

$$\hat{S}_i = \mathbf{w}_i^H \mathbf{p}, \tag{15}$$

with ^{H} the conjugate transpose operation and

$$\mathbf{w}_i = \frac{1}{M}\begin{bmatrix} \exp(-j2\pi f\tau_{1i}) \\ \vdots \\ \exp(-j2\pi f\tau_{mi}) \\ \vdots \\ \exp(-j2\pi f\tau_{Mi}) \end{bmatrix} \tag{16}$$

the steering vector. To reduce the statistical bias, the square power of the estimation is averaged over a 20 Hz frequency bandwith.
In fact, beamforming is based on the hypothesis of plane wave and the compensation of the propagation effects. It performs a spatial filtering in the focussing direction $[\theta_i\ \phi_i]$; the spatial filtering properties depends strongly on the geometry of the array (*i.e.* the spatial repartition of the sensors) [8]. For a harmonic source at 800 Hz coming from the DOA equal to 0 °, beamforming processing provides the estimation of the sound radiation in Figure 8. The maximum indicates the source position, it becomes wider at low frequencies and the detection is less accurate. Ghost sources with no physical reality are created by beamforming, which could lead to misinterpretations. The microphone placements are optimized on a 3 m by 3 m grid, 40 microphones are used. The optimization leads to an asymmetrical placement of microphones so is the DOA detection.

4 Application to the rail model

As mentioned above, beamforming can identify source locations. It seems to be an adapted solution for characterizing the radiation angle of the rail. In our case, simulations are run using a 2D array developped by SNCF for acoustic mapping of the train. Linear arrays were used in previous investigations [4, 7]. Simulation conditions are the same as in real pass-by condition: the rail model is placed 4m in front of the array and 2 m below the center.
Two excitation positions are tested. First, the excitation is done in front of the center of the array, the position angle

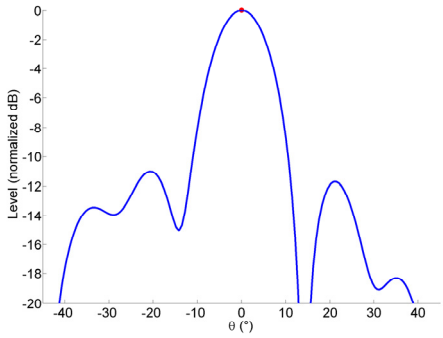

Figure 8: Localization of a harmonic source at 800 Hz using beamforming processing with an optimized array geometry of 40 sensors. The DOA of the source is 0 ° (red point).

with regard to the center of the array is $\theta_e = 0$ °. Then, the excitation is done at $\theta_e = -30$ °. The elevation of the rail is $\phi_e = -63$ ° from the center of the array. The model is run for the [200 1200] Hz band (this is the frequency band of the array).

Beamforming is performed along the rail and a frequency versus angle map indicates the variation of the incoming angle. The results from $\theta_e = 0$ ° are presented in Figure 9, the theoretical angle is plotted in a continuous red line and the excitation position in the black dashed line. The main contribution is located of the excitation at 0 °.

When the excitation is changed to $\theta_e = -30$ °, beamforming

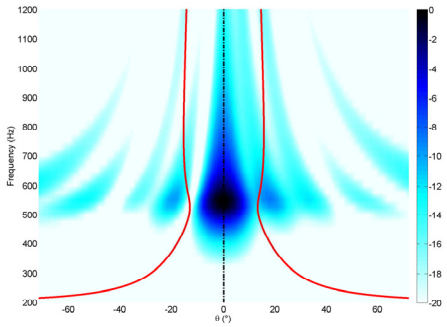

Figure 9: Detection of the direction of arrival for the rail model. The excitation is located at 0 ° (black line) and the theoretical angle, θ_0, is in red.

processing identifies the DOA of the theoretical angle in Figure 10. Around 500 Hz, it is difficult to detect the theoretical radiation angle, as beamforming is less accurate at low frequencies. In addition, the attenuation coefficient of the wave is still important as shown in Figure 3, the assumption to replace the rail with a monopole line is not relevant.

For both cases, several ghost sources appear and the location of the theoretical angle is not accurate.

These beamforming simulations based on the rail model highlight some conditions to detect the theoretical angle θ_0:

- the attenuation coefficient α of the waves in the rail should be low enough to validate the monopole line hypothesis;
- the position angle θ_e should be greater than the radiation angle θ_0.

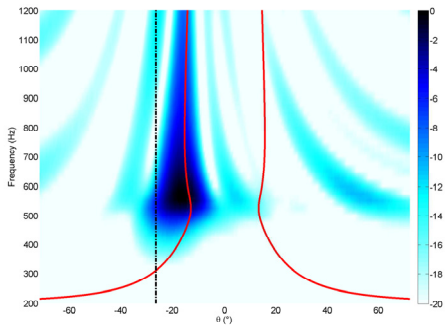

Figure 10: Detection of the direction of arrival for the rail model. The excitation is located at -30 ° (black line) and the theoretical angle, θ_0, is in red.

5 Experiment

The characterization of the rail radiation was performed during a measurement campaign on a French high speed line.

5.1 Set-up

The rail is located 4 m and -2 m lower than the array center. The lowest sensors of the array are located at the rail height. The rail was excited using an encapsulated shaker to reduce the noise generation (see Figure 11). The shaker is driven by a white noise signal in the [200 2000] Hz frequency band. Two excitation positions are tested: 0 ° and -30 °, as for the simulations.

A characterization of the track was performed in 2008 by

Figure 11: Encapsulated shaker.

the SNCF test departement [9]. The measured accelerance is represented in Figure 12. Its highest value is at 1100 Hz, this is the pinned-pinned frequency due to the sleeper periodicity. Despite this difference, the measured accelerance is closed to the simulated one in Figure 4.

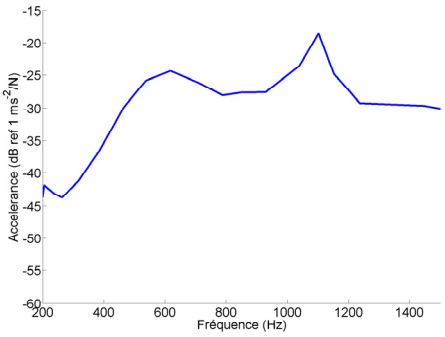

Figure 12: Measured accelerance in the vertical direction.

5.2 Results

The DOA versus frequency map for the 0 ° excitation is plotted in Figure 13. The simulation showed that the source is located at 0 ° but the experiment results show sources all along the rail with higher level at low frequencies. Moreover, the map is noisy.

When the excitation is placed at -30 °, contrary to Figure 10,

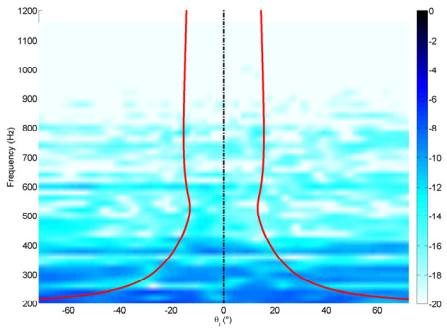

Figure 13: Detection of the direction of arrival for the rail. The rail is excitated in 0 ° (black line) and the theoretical angle is in red.

the theoretical radiation angle is not retrieved in Figure 13. As for the 0 ° excitation, the main sources are located all along the rail and particularly at low frequencies.

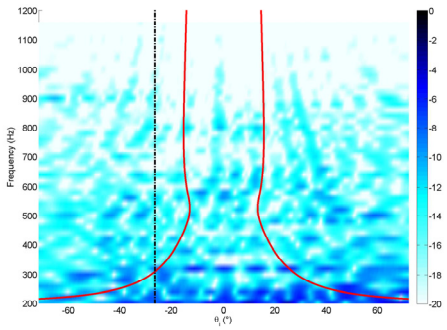

Figure 14: Detection of the direction of arrival for the rail. The rail is excited in -30 ° (black line) and the theoretical angle is in red.

Conclusions and perspectives

Beamforming does not identify the rail as a main source on acoustic maps of the train even if theoretical predictions indicate that it is an important contribution to the rolling noise. A simple rail radiation model previously developed is introduced to explain this underestimation of the rail noise level. This model is based on physical parameters of the track. The rail is composed of a monopole line, which amplitudes are linked to the loss factor of the bending wave and the mobility of the rail. A particular direction of radiation is observed. Beamforming processing is able to find this direction only under specific conditions: the position angle of the excitation should be greater than the radiation angle and the attenuation of the wave in the rail should be low enough.

An experiment is conducted on a French railway track, using a shaker and an array designed for source localsiation on the train. The experimental results are not correlated to the simulation predictions. The theoretical angle is not retrieved and maps are highly polluted at low frequencies. High resolution array processing developped in [7] seems to be more adapted for the radiation angle detection.

On one hand, the array used is assumed to be not adapted to identify the theoretical angle and linear arrays seem to be more revelant. On the other hand, a more complex model should be developped to understand the 3D sound field radiated by the rail, as the study of a FEM rail model radiation presented in [10].

References

[1] D. J. Thompson, "Wheel-rail noise: theoretical modelling of the generation of vibrations", *PhD thesis, University of Southampton*, (1990)

[2] D. J. Thompson, "Railway noise and vibration", *Elsevier*, First Edition (2009)

[3] F. Poisson, "Localisation et caractérisation de sources acoustiques en mouvement rapide", *PhD Thesis, Université du Maine*, (1995)

[4] T. Kitagawa, D. J. Thompson, "The horizontal directivity of noise radiated by a rail and implications for the Use of microphone arrays", *Journal of Sound and Vibration* **329**, 202-220 (2010)

[5] T. Kitagawa, "An Investigation into Inconsistencies between theoretical predictions and microphone array measurements of railway rolling noise", *PhD thesis, University of Southampton*, (2007)

[6] D. J. Thompson, J. Mahe, P. Fodiman, "Experimental validation of the TWINS prediction program for the rolling noise, part 2: results", *Journal of Sound and Vibrations* **193(1)**, 137-147 (1996)

[7] B. Faure, "Caractérisation du rayonnement acoustique d'un rail à l'aide d'un réseau de microphones", *PhD thesis, Université de Grenoble* (2011)

[8] F. Le Courtois, J.-C. Pascal, F. Poisson, J.-H. Thomas, "Optimisation par algorithme génétique de la géométrie d'antenne pour la localisation de sources", *Congrès Français d Acoustique, Lyon* (2008)

[9] C. Tiphonnet, C. Mellet, F. Létourneaux, "Caractérisation acoustique du site de mesure au passage", *SNCF technical report* (2008)

[10] L. Gravić, "Calcul de propagation des vibrations dans un rail libre", *Journal de physique III* **4**, 73 (1994)